Low dimensional hollow nanostructures: from morphology control to the release of an active pharmaceutical ingredient

Loraine Soumoy[1], Luca Fusaro[1], Damien P. Debecker[2], Carmela Aprile[1]*

[1]University of Namur, Laboratory of Applied Materials Chemistry, Unit of Nanomaterials Chemistry, Department of Chemistry, NISM, 5000 Namur, Belgium

[2]Université catholique de Louvain (UCLouvain), Institute of Condensed Matter and Nanosciences (IMCN), 1348 Louvain-la-Neuve, Belgium

** Corresponding author: carmela.aprile@unamur.be*

ABSTRACT

The mechanism guiding the growth of hollow silica nanotubes or nanospheres was unveiled for the first time through in situ liquid-phase transmission electron microscopy, allowing visualization of the morphology of the hydrated species involved in the early stage of material formation. The combined action of a surfactant (F127) and a swelling agent (toluene) was essential for the development of targeted nanostructures, owing to the formation of surfactant-stabilized toluene droplets in the aqueous phase. The quantity of surfactant-stabilized toluene droplets was unambiguously pointed as the key parameter guiding the formation of either tubular or spherical nanostructures. Leveraging on the fundamental understanding of the parameters guiding the formation of hollow silica nanostructures, tubular and spherical carriers were prepared and exploited for the release of an active pharmaceutical ingredient (API). The impregnation of nanotubes and nanospheres with a poorly watersoluble API (curcumin) was investigated, leading to an optimal loading of 20 wt %. The accessibility of nanotubes and nanospheres showed to be highly beneficial to increase the release kinetics of the targeted API in simulated intestinal fluid, opening promising perspectives in the field. Release was more efficient than with other conventional mesoporous silica-based carriers.

Over the past decades, micelle-templated strategies were exploited to synthesize a myriad of porous silica-based materials displaying various pore sizes and morphologies.[1-4] Despite significant advancements, the fundamental mechanisms of the formation of micelle-templated solids is constantly attracting the attention of the entire scientific community. In 2004, first experimental evidence on the progression of micelle-TMOS aggregation provided insights into the formation mechanism of the mesoporous silicate with SBA-15 structure.[5] Other studies dealing with the formation mechanism of mesoporous solids as KCC-1[6] or aminated surfactant-templated mesoporous silica[7] were undertaken as well.

Recently, hollow silica-based nanotubes and nanospheres emerged as highly appealing structures within the broad family of mesoporous silica-based materials.[8] Their highly-open structure, elevate specific surface area and large pore diameter proved to be favorable features for catalytic applications.[9, 10] Interestingly, their synthesis protocol involves a single combination of silica precursor, surfactant and swelling agent able to template the two distinct morphologies as function of the condition employed.[8] By inspecting the synthesis procedure, the only parameters identified as significantly different are the stirring speed and the time between the addition of the swelling agent (toluene) and the silica precursor (tetraethyl orthosilicate, TEOS). In particular, the synthesis of nanotubes takes place at 250 rpm with a simultaneous addition of toluene and TEOS (see experimental and Figure 1 for more details). For the synthesis of nanospheres, the stirring speed is increased to 350 rpm and the addition of TEOS is delayed by 24h after the toluene addition (Figure 1). Previous works hypothesized that the formation of hollow nanospheres occurs via the fragmentation of nanotubes, through a budding process.[8, 11] Nevertheless, no precise experimental evidence concerning the overall mechanism of nanotubes/spheres formation was described until now.

In-depth understanding of the formation mechanisms of hollow silica nanotubes/spheres will represent a fundamental advancement and will undoubtedly allow a better control of their morphology. Independently from the selected application, the morphology of a material is one of the key features that must be accurately controlled. In the field of catalysis, the morphology of nanotubes has already shown to be highly beneficial for the conversion of glycerol into solketal.[9, 10] In the field of drug delivery, the topology/structure and diameter of the pores of the carrier have already shown to play a major role on the dissolution rate of poorly-water soluble drugs. In particular, the enhancement of dissolution rate was associated with the improvement of the diffusion properties of the carrier.[12, 13]

Since their discovery in 1990, mesostructured silica-based materials have been subjected to intense research for their application in the pharmaceutical field as delivery carriers for active pharmaceutical ingredients (API).[14-17] Their large specific surface area together with their high content of surface silanol allow the preparation of a myriad of functionalized porous silicates presenting high loadings of active molecules. Thus, mesostructured silica-based solids are employed to enhance the dissolution rate of poorly water-soluble APIs (s < 100 µg/mL).[18] This category of APIs represent about 90% of the new drug candidates and 40% of the commercially available drugs. The problem of low solubility in water is even more pronounced for promising natural products or phytochemicals (curcumin, apigenin, etc.), that are mostly lyophilic. Despite their high potential (e.g., antibacterial, antioxidant, anti-inflammatory properties[19, 20]), their low dissolution kinetic drastically limits the direct pharmaceutical application. Solid dispersion[21], encapsulation in mesoporous silica[18, 22] or crystal engineering[23, 24] are well-known techniques to achieve dissolution rate enhancement. The encapsulation of APIs in the pores of mesoporous silicates such as MCM-41 or SBA-15 has already allowed excellent in-vitro and in-vivo dissolution rate enhancements.[25, 26] The phenomenon can be associated with the stabilization of the API in the amorphous phase together with the fact that recrystallization is hampered due to finite size effects and favorable surface H-bonding. The development of new silica-based vehicles presenting an architecture allowing both stabilizing the active amorphous phase and avoiding diffusion limitations represents a topic of great interest. The mesoporosity and the highly open structure of hollow nanospheres and nanotubes seems very promising to achieve considerable release rate enhancements of the poorly water-soluble curcumin.[8]

In this contribution, we precisely identified the synthesis parameters guiding the development of the hollow tubular and spherical morphologies. To the best of our knowledge, the proper identification of the key parameter(s) leading to the formation of the two distinct architectures was never systematically undertaken. The careful study of these parameters together with an in-depth characterization of the morphology and textural properties of these micelle-templated solids allows unveiling the formation mechanism of both nanotubes and nanospheres. Nanotubes and nanospheres were impregnated with the poorly water-soluble curcumin. Nanotubes and especially nanospheres showed to be particularly efficient carrier if compared to pristine commercial curcumin or even with more common mesoporous silica-based carriers reported in the literature.

RESULTS AND DISCUSSION

Parameters influencing the tube-to-sphere transition

The procedure reported in Figure 1 was selected as starting point for the investigation of the formation mechanism of hollow nanotubes and nanospheres. It is important to note that this synthesis strategy is an optimization of the procedure previously reported by Kruk et al [8] and includes a pH adjusting step that replaces the traditional hydrothermal treatment under static conditions. This approach was successfully employed by us for the synthesis of Hf-doped silica nanotubes.[9]

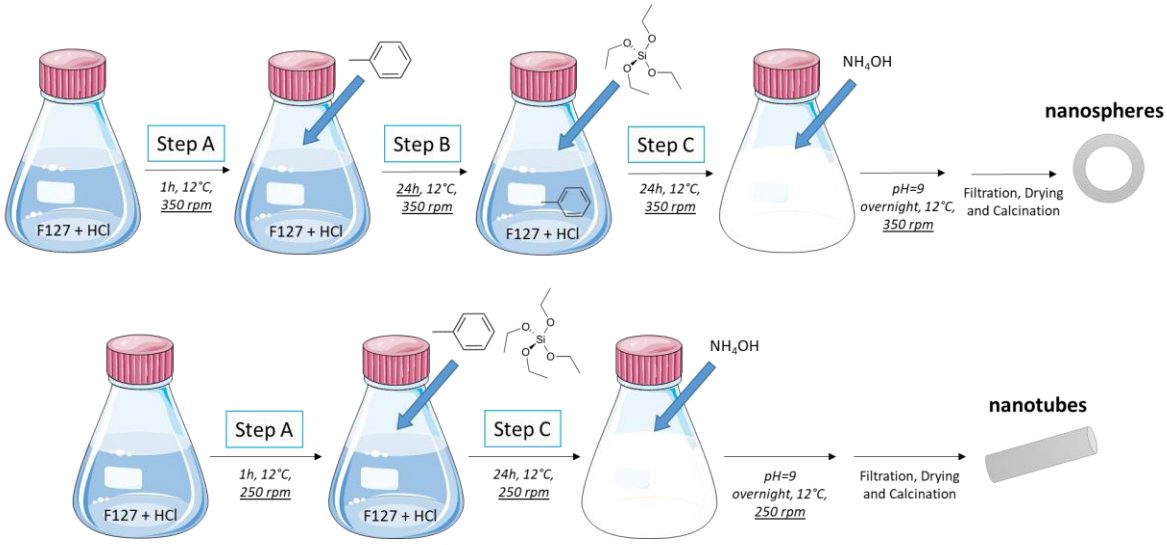

Figure 1 – Procedures for the synthesis of silica-based nanospheres and nanotubes inspired from the literature.[8, 9] The differences between the two procedures were underlined. Synthesis conditions: 1.0 g of F127, 60.0 mL of HCl 2M, 3.0 mL of toluene, 2.8 g of TEOS and 10.5 mL of NH_4OH 30 wt.%. The figure was partly generated using Servier Medical Art, provided by Servier, licensed under a Creative Commons Attribution 3.0 unported license.

The careful observation of the experimental protocols for the synthesis of hollow silica-based nanotubes and nanospheres reveals the presence of various identical steps (Figure 1).[8] Considering the preparation of hollow silica nanotubes as a starting point (bottom of Figure 1), we attempt to elucidate the key parameters guiding the synthesis towards either nanotubes or nanospheres. Thus, hollow silica nanotubes were prepared with a stirring speed of 250 rpm and without delay time ($\Delta t = 0$ h) between the addition of toluene and TEOS (see experimental section for more information). A series of three materials was subsequently prepared by increasing Δt to 2 h, 8 h and 24 h. Another series of materials was synthesized by increasing the stirring speed to 350 rpm, 450 rpm and 550 rpm while preserving $\Delta t = 0$ h. The two parameters were modulated separately to study their impact on the textural and morphological properties of the solids. The solids were named indicating both the delay time between the addition of

toluene and TEOS (Δt = 0 h, 2 h, 8 h, 24 h) and the stirring speed employed during their synthesis (250 rpm, 350 rpm, 450 rpm, 550 rpm).

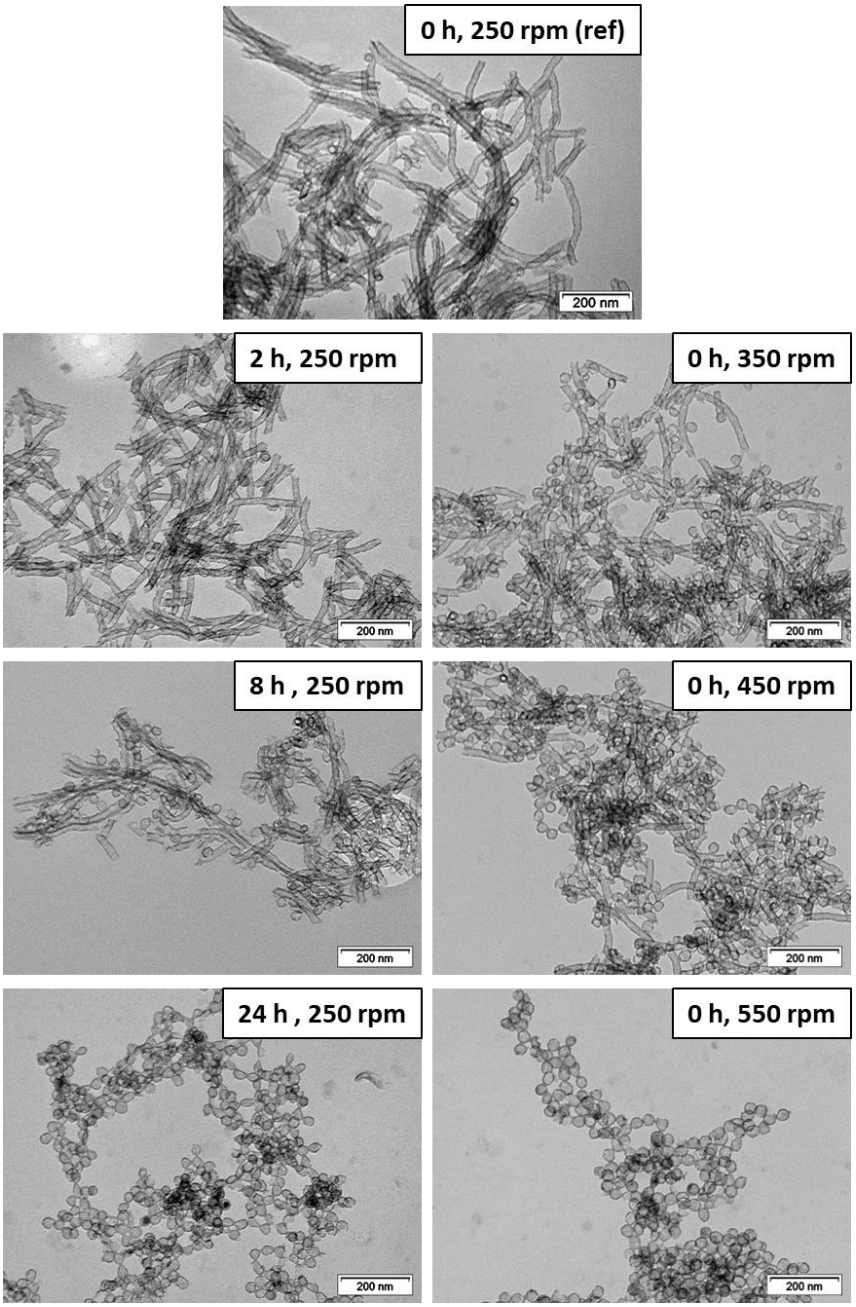

Figure 2 – TEM micrographs of as-synthesized hollow nanostructures synthesized using different delays between the addition of toluene and TEOS (left) or different stirring speed (right).

The morphology of the materials was investigated via transmission electron microscopy (TEM, Figure 2). The reference solid (0 h, 250 rpm) was homogeneously constituted of well-defined tubes with clearly visible walls and internal voids, in agreement with previous reports.[8] The tubular structures were mostly

separated in loose aggregates without any organization or periodicity. The diameter of the tubes was estimated to be around 22 nm. No difference was evidenced inspecting the sample prepared with Δt = 2 h (2 h, 250 rpm). Interestingly, when Δt was increased to 8 h, the presence of some isolated hollow nanospheres was clearly detected. When a Δt = 24 h was employed, only well-defined hollow nanospheres were visible, throughout the sample. TEM investigation of the samples synthesized by varying exclusively the stirring speed (and maintaining Δt = 0 h) reveals the appearance of hollow nanospheres together with well-defined tubular structures when the stirring speed was increased from 250 rpm to 350 rpm or 450 rpm (0h, 350 rpm and 0h, 450 rpm). A further increase in the stirring speed (0h, 550 rpm) allowed obtaining a sample constituted only by nanospheres with a diameter of *ca.* 30 nm. The syntheses of nanotubes and nanospheres were repeated twice with highly reproducible results. It should be noted that the procedure employed to prepare the last solid (0h, 550 rpm) represents the best strategy (uniform morphology and limited time) to obtain a material containing only hollow particles with a spherical morphology.

The inspection of calcined nanotubes and nanospheres via high resolution TEM (HR-TEM, Figure 3) allowed evaluating the thickness of the walls that lies between 3-4 nm for both hollow nanostructures. HR-TEM micrographs show also the presence of small pores (indicated with white arrows in Figure 3b, d) in the shell of the materials. The latter can be considered as micropores (< 2 nm) probably generated by the interpenetration of some polyethylene oxide (PEO) chains of the templating agent (PEO_{100}-PPO_{65}-PEO_{100}) through the silica walls. However, a careful analysis of HR-TEM micrographs evidence, in a minor amount, some light grey spots (black arrows in Figure 3b, d) of irregular shapes in the shell of both nanostructures, suggesting the presence of wider pores. The exact size of these zones is difficult to evaluate due to their non-circular shape, but we can estimate that the largest measure about 5 nm.

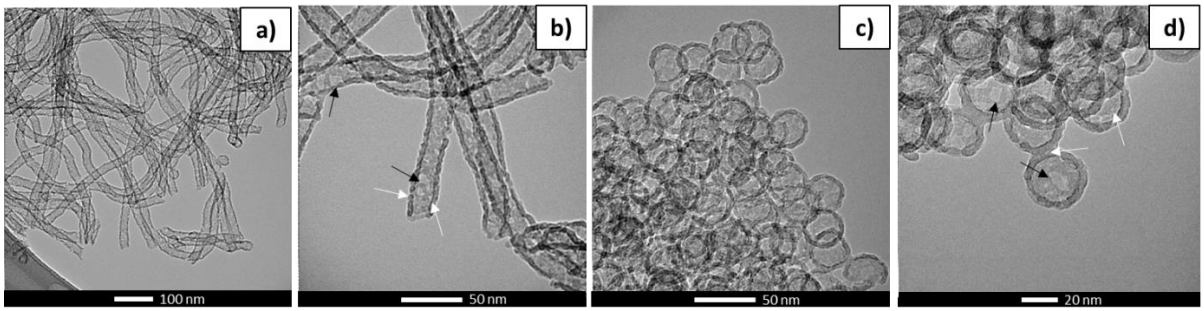

Figure 3 – HR-TEM of calcined nanotubes a, b) and calcined nanospheres c, d). White arrows highlight the presence of small pores in the shell of nanotubes and nanospheres and black arrows could indicate the presence of larger gaps in their shell.

The textural properties of the solids were investigated via N_2 adsorption-desorption analysis. The isotherms reported in Figure 4 show the presence of a sharp nitrogen uptake at low relative pressure (close to 0.02), indicating the presence of micropores. The capillary condensation appearing at high relative pressure (around 0.8) can be ascribed to the presence of large mesopores, as revealed by TEM analysis. The reference solid (0 h, 250 rpm) as well as the (2 h, 250 rpm), (8 h, 250 rpm), (0 h, 350 rpm) and (0 h, 450 rpm) materials, present a capillary condensation including two distinct steps which can be considered as a combination of (i) the filling of particle interiors at lower P/P_0 and (ii) the filling of the interparticle voids at higher P/P_0. Interestingly, the narrow hysteresis loop together with the presence of a tail (toward a relative pressure of around 0.7), indicate that most pores were accessible without any major constrictions.[8] Both nanotubes and nanospheres exhibit a high specific surface area (Brunauer, Emmett et Teller, BET) of about 600 m^2/g and a large total pore volume of about 2 cm^3/g (Table 1). Mean pore diameters were evaluated with the Barrett-Joyner-Halenda (BJH) method, using the Kruk-Jaroniec-Sayari (KJS) correction[27] and lies between 19 and 27 nm. The pore size distribution (Figure S1) expands towards higher pore diameter when passing from tubular to spherical structures, in accordance with TEM observations.

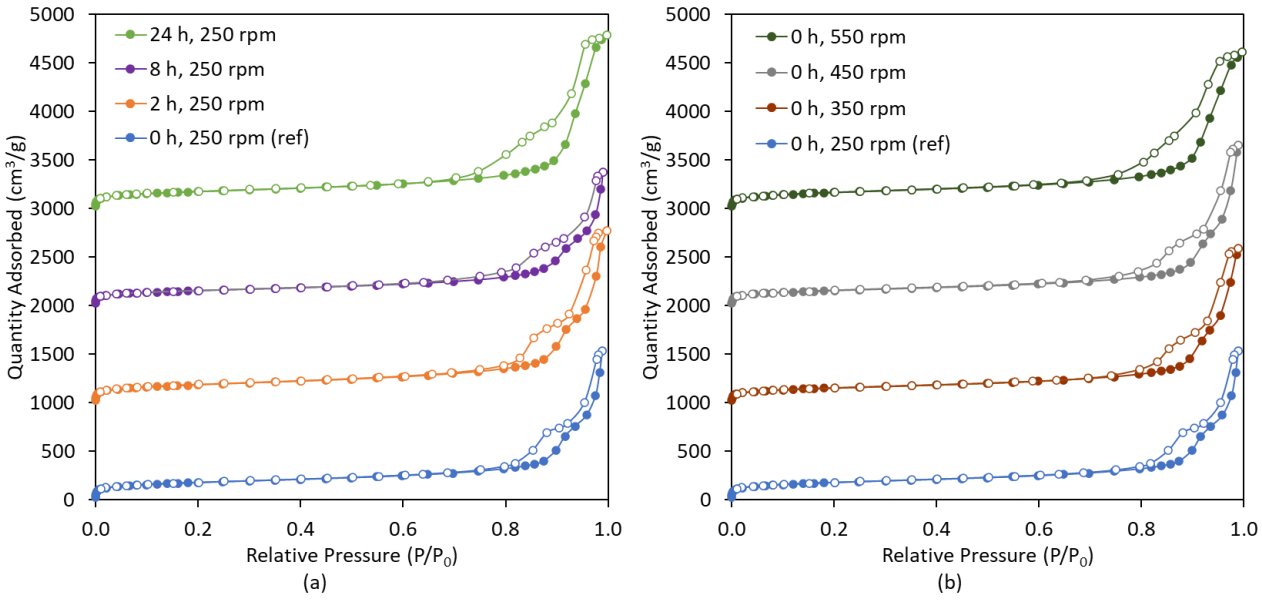

Figure 4 – Adsorption-desorption N_2 isotherms of hollow nanostructures synthesized with different delays between the addition of toluene and TEOS (a) and different stirring speeds (b). For clarity, some isotherms were shifted to 1000, 2000 or 3000 cm^3/g.

Table 1 – Textural properties of solids synthesized under different stirring speeds or time between addition of toluene and TEOS

Entry	Time between toluene and TEOS (h)	Stirring speed (rpm)	BET SSA (m^2/g)	MPD BJH (nm)	V_t (cm^3/g)
1	0	250	640	22	2.4
2	2	250	660	22	2.5
4	8	250	560	19	2.1
5	24	250	550	27	2.5
7	0	350	580	22	2.5
8	0	450	550	22	2.4
9	0	550	600	23	2.4

Investigating the formation mechanism of nanotubes and nanospheres

The above-mentioned observations reveal that the addition of toluene and TEOS within an interval of 2 hours (Δt = 0 h or 2 h), together with the application of a gentle shearing force (250 rpm) lead to the formation of nanotubes. Moreover, increasing the time between the addition of toluene and TEOS to 24 h or enhancing the stirring speed to 550 rpm always yield hollow nanospheres. Thus, we identified the parameters guiding the formation of nanotubes or nanospheres. To go deeper, we attempted to elucidate the mechanisms that stir the system toward the formation of either tubular or spherical hollow nanostructures.

Previous work hypothesized that the formation of hollow nanospheres occurs via the fragmentation of pre-formed nanotubes, through a budding process.[8, 11] In order to test this hypothesis, additional syntheses were performed by varying the stirring speed from 250 rpm to 550 rpm, 2, 4 or 8 hours after the simultaneous addition (0 h) of TEOS and toluene (see experimental and Figure S2 for details). In the first part of the experiment, a stirring speed of 250 rpm was employed to allow generating a certain amount of silica nanotubes. In the second part of the experiment, an intense shirring force (550 rpm) was applied to check if the formation of nanospheres can be the result of a fragmentation of nanotubular species. TEM micrographs on these new samples revealed the presence of well-defined nanotubes with only a marginal presence of nanospheres (Figure 5) thus indicating that the tube-to-sphere transition did not occur predominantly via the fragmentation of pre-existing tubular structures.

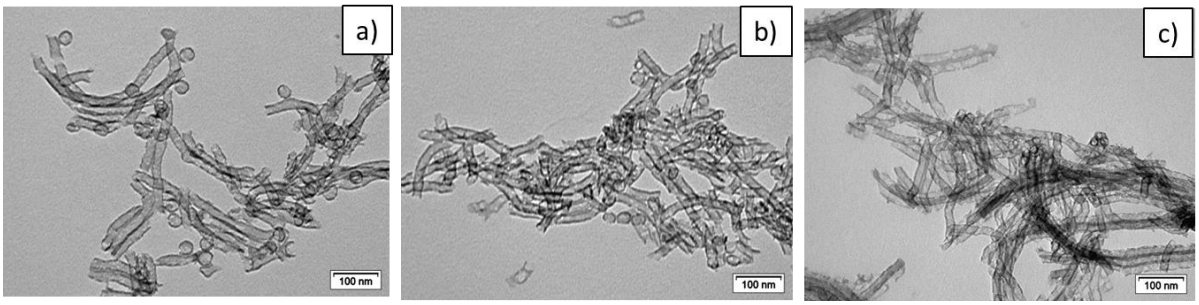

Figure 5 - TEM micrographs of samples synthesized by varying the stirring speed from 250 rpm to 550 rpm 2h (a), 4h (b) and 8h (c) after the simultaneous addition of toluene and TEOS.

To shed more light on the mechanisms guiding the formation of nanotubes/spheres, a stepwise investigation was performed. The mixture of solubilized F127 (step A, on Figure 1) was analyzed via differential light scattering (DLS, Figure S3a). The DLS analysis revealed that the solution was composed of species displaying a hydrodynamic diameter centered at 6 nm, whatever the stirring speed applied. The size of the species is consistent with the presence of F127 unimers[28] and indicates that the critical conditions for the formation of micelles with well-defined geometries were not reached in the first step of the synthesis procedure. Hence, the key event responsible of the formation of nanotubes or nanospheres should most probably occur in step B.

The next step of the procedure (step B) implies the addition of toluene (3 mL) in the solution of solubilized F127 at 12°C. To investigate the role of toluene in the proposed synthesis protocol, a solid was synthesized by omitting the addition of this swelling agent (see experimental for details). TEM and N_2 physisorption analysis (Figure S4 and S5) reveal the presence of a mesoporous solid (SSA of 410 m^2/g, total pore volume of 0.7 cm^3/g and MPD BJH-KJS of 8 nm) that is mostly disorganized and displays an ill-defined morphology. This experiment highlighted that the use of toluene is crucial for the synthesis of hollow nanostructures with well-defined morphologies.

To better understand the role of toluene in the formation mechanism of nanotubes and nanospheres, the synthesis mixture at the step B (Figure 1) was analyzed. The mixture was analyzed 2 hours and 24 hours after the addition of toluene at 12°C, 250 rpm to be consistent with the development of the tubular (2 h, 250 rpm) and spherical (24 h, 250 rpm) morphology (*vide supra* and Figure 2). The visual observation of the mixture 2 h after the addition of toluene showed the presence of two translucent phases (Figure S6). The upper phase was mostly composed of toluene (lyophilic phase) while the bottom phase was mostly composed of acidified water (aqueous phase). After 24 h, the biphasic system evolved towards a cloudy sol (Figure S6). The increased turbidity of the mixture accompanied by the disappearance of the two

distinct phases could be ascribed to the progressive dispersion of toluene (stabilized by the F127 surfactant) in the aqueous phase, i.e. forming an oil-in-water emulsions.[29, 30]

To support our hypothesis, the two samples were analyzed via DLS. DLS performed on the aqueous phase (main phase) revealed the presence of a wide distribution of hydrodynamic diameters (until ≈ 200 nm of width) with a maximum intensity at 61 nm and 46 nm, for the sample collected after 2 hours and 24 hours, respectively (Figure S3b). On the one side, from this study emerges the presence of new species in the aqueous phase with larger diameter. These species are most probably constituted by toluene droplets surrounded by a shell rich in F127. On the other side, the large width of the distribution could be attributed to different phenomena such as the presence of species with a broad size distribution or the coexistence of various morphologies.[31]

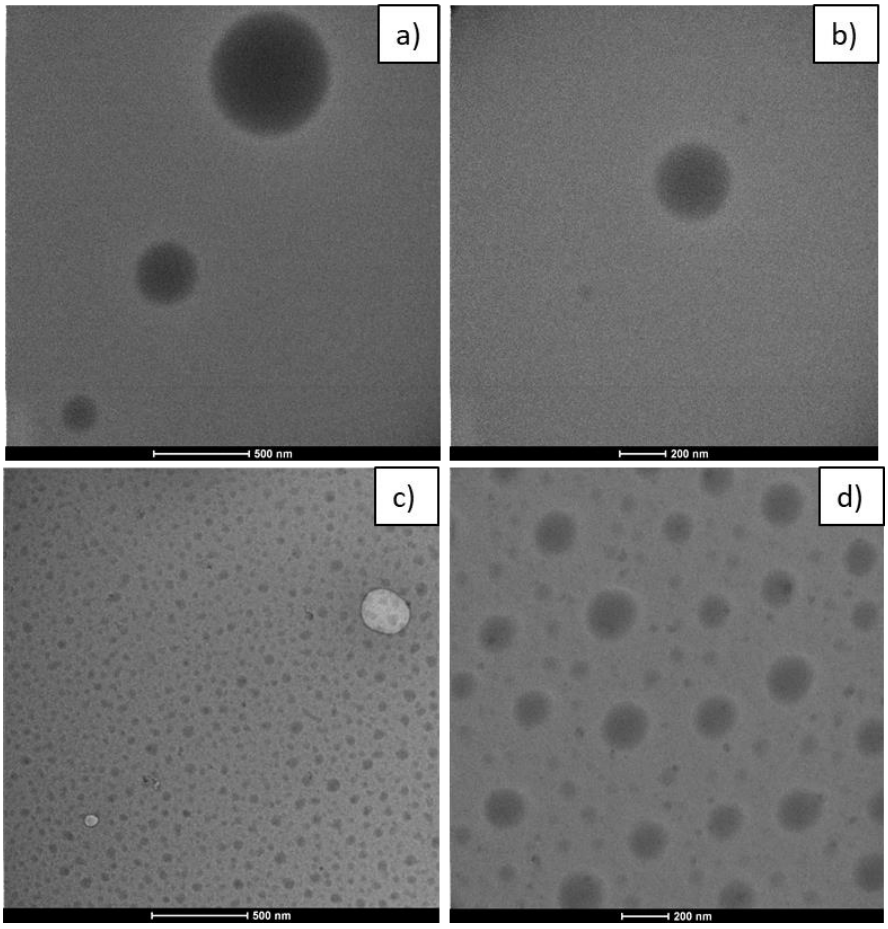

Figure 6 - Liquid-phase transmission electron microscopy of 1.0 g of F127, 60.0 mL of HCl 2M and 3 mL of toluene after 2 hours (a,b) and 24 hours stirring (c,b) at 250 rpm, 12°C.

Hence, the samples of the aqueous phase collected 2 hours and 24 hours after the addition of toluene were analyzed via liquid-phase (LP)-TEM. This technique allows analyzing samples that are fully hydrated in their native liquid media without the need of drying or vitrifying the specimen. Very recently, the advances in liquid cell fabrication put the LP-TEM under the spot light as a powerful tool to study a wide range of nanoscale processes occurring in solution that were previously out of reach. LP-TEM can be hence considered as an emergent platform to study, *inter alia*, soft matter in solution. [32-36]

LP-TEM observation of a small fraction of the aqueous phase collected 2 h after toluene addition reveals the presence of some spherical droplets with a diameter above 150 nm (Figure 6a, b) together with a low amount of much smaller droplets presenting a diameter around 40 nm. After 24 h stirring (Figure 6c, d), LP-TEM analysis of a small fraction of the mixture reveals the presence of a completely different pattern; a higher quantity of smaller spherical droplets (40-60 nm of diameter) was clearly observed. Interestingly, LP-TEM observations are highly consistent with the hypothesis deduced from the visual observations of the synthesis mixture (*vide supra*).

The above-mentioned results revealed that the presence of surfactant-stabilized toluene droplets play a pivotal role in the development of the nanotubes and nanospheres structures. In particular, the amount of dispersed toluene could be the « true » key parameter orienting the synthesis toward the formation of either nanotubes or nanospheres. In the case of nanotubes, due to the gentle stirring (250 rpm) or to the simultaneous addition of toluene and TEOS, not all the added toluene molecules could be involved as swelling agent in the formation of the template and a part of them remains as a separate phase.

If this hypothesis is correct, the presence of a limited amount of toluene under the conditions leading to the formation of silica nanospheres (24 h, 250 rpm) should instead produce silica nanotubes (see experimental and Figure S7 for details). To test this hypothesis, a synthesis was performed by adding a lower amount of toluene (1 mL) than the quantity used in the synthesis of nanospheres (3 mL). It is important to note that the addition of TEOS was performed after 24 h to favor the incorporation of toluene in the aqueous phase of the reaction mixture. Interestingly, the analysis of the solid via TEM reveals the presence of tubular structures (Figure S8). This observation confirms the crucial role of toluene (or more precisely of the amount of toluene dispersed in the aqueous phase in the form of surfactant-stabilized droplets) in the creation of hollow nanostructures with distinct morphologies.

In the case of nanospheres, the development of the spherical morphology could be related to the presence of a high quantity of stabilized toluene droplets in the aqueous phase due to the intense stirring

(0 h, 550 rpm) or the prolongated stirring of toluene (24 h, 250 rpm). To test this hypothesis, a mixture of F127, HCl 2M and toluene (steps A and B, Figure 1) was vigorously stirred at 1000 rpm for 2 hours to favor the incorporation of toluene in the aqueous phase. Then, the stirring speed was reduced to 250 rpm for the addition of TEOS. The TEM analysis of the resulting solid revealed the presence of hollow nanospheres (Figure S9). The same synthesis mixture led to the formation of nanotubes when a stirring speed of 250 rpm was used during all the procedure (see solid named 2 h, 250 rpm in Figure 2). This observation strengthens the fundamental importance of toluene droplets to guide the formation of the desired morphology.

The formation of mesoporous structured silicates involves both the pre-organization of the template and the formation of a silica framework around this template. To investigate if the hydrolysis of the silica precursor (TEOS) could influence the formation of nanotubes and nanospheres, the rate of TEOS hydrolysis was investigated through ^{1}H NMR experiments.[37] A preliminary study aiming at the proper identification of the NMR signals is described in the supporting information (Figure S10-S14). The experiments were performed in triplicate, on a mixture simulating the synthesis of nanotubes (0 h, 250 rpm) or nanospheres (24 h, 250 rpm). Detailed information can be found in the experimental section. Since the hydrolysis of TEOS led to the release of ethanol, the evolution of the corresponding -CH_2 signal was followed as a function of time. Figure 7a shows the relative increase of the EtOH signal (-CH_2, 2.9-3.0 ppm) with respect to the F127 signal (-CH_2 of the PEO block, 3.0-3.1 ppm) in the case of nanospheres. The evolution of TEOS hydrolysis for nanotubes and nanospheres is illustrated in Figure 7b. In both cases, the amount of EtOH increases rapidly during the first 15 minutes following TEOS addition, after which a stabilization of the released ethanol is observed. After 45 minutes, the EtOH(-CH_2)/F127(-CH_2 PEO) molar ratio reached a value included between 1.5 and 1.6 which is closed to the theoretical value of 1.7. One hour after the addition of TEOS (Figure 7a), the NMR signals become broader as a consequence of increased viscosity, attributed to the formation of polymeric silica species, and poor magnetic field homogeneity. A similar rate of TEOS hydrolysis is evidenced for both nanotubes and nanospheres. This indicates that the TEOS hydrolysis rate is not the key parameter that governs the formation of either spheres or tubes, and instead supports our conclusion on the essential role of toluene droplets.

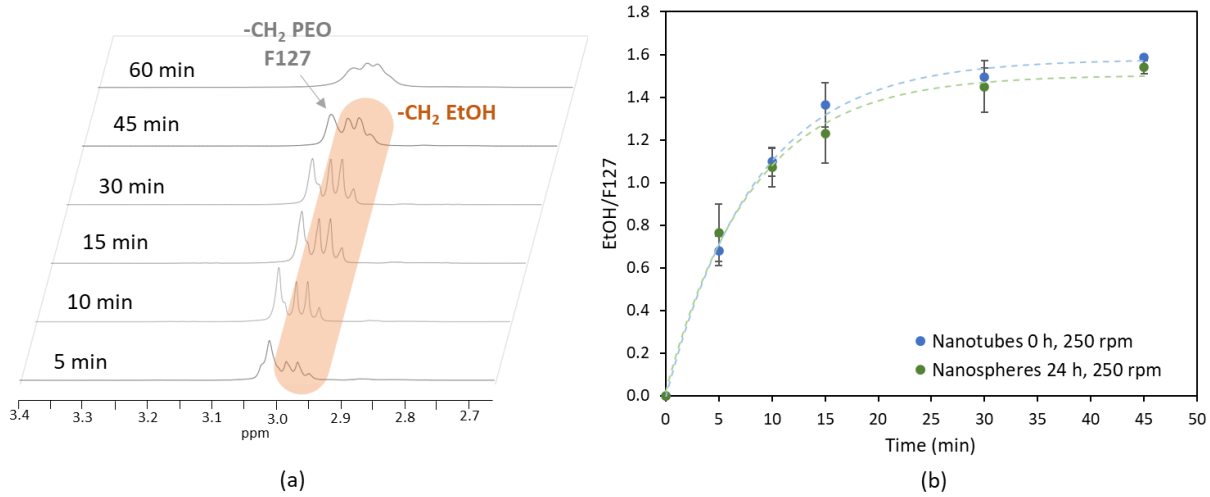

Figure 7 – Evolution with time of ^{1}H NMR spectra (2.7 ppm – 3.4 ppm) of a mixture used for the synthesis of nanospheres after TEOS addition (a) and evolution of the ratio between the -CH_2 signal of EtOH and the -CH_2 signal of the PEO block of F127 with time.

All the previous investigations led us to propose a mechanism that can explain the growth of either tubular or spherical structures (Figure 8). The shearing force induced by the stirring allows generating surfactant-stabilized toluene droplets in the aqueous phase. The silica source, mainly located in the oil phase, undergoes hydrolysis at the oil-water interface to yield hydroxylated species and ethanol that arrange in the proximity of the hydrophilic moieties and diffuse in the aqueous phase.[38, 39] At pH 0 (pH of the synthesis mixture), hydroxylated silica species will probably quickly react to yield silica oligomers.[40] Due to the stirring of the mixture, silica species can reach the surfactant-stabilized toluene droplets and interact via hydrogen bonding with the PEO part of the copolymer block.

In case of a high number of stabilized toluene droplets (intense shearing force), we can assume that a major part of toluene and F127 are involved in the stabilization of the toluene droplets in the aqueous phase. The silica oligomers will start to simultaneously interact with many toluene-stabilized droplet, depleting the reserve of silica oligomers. As consequence, the condensation arises in the periphery of the stabilized toluene droplets, leading to spherical particles. On the contrary, if the number of stabilized toluene droplets is low (gentle shearing force), we can assume that a part of the reactants (copolymer block F127, toluene and silica oligomers) does not participate to the creation of stabilized toluene droplets in the aqueous phase. Hence, a part of the reactants is still available in the reaction mixture to further react/interact and finally lead to the development of nanotubes. Since the development of tubular structures is less evident at this stage, we surmise that the chemical nature of TEOS or more precisely, its

hydrolyzed products (ethanol, silica oligomers), should probably play an active role in the formation of the final nanotubes.

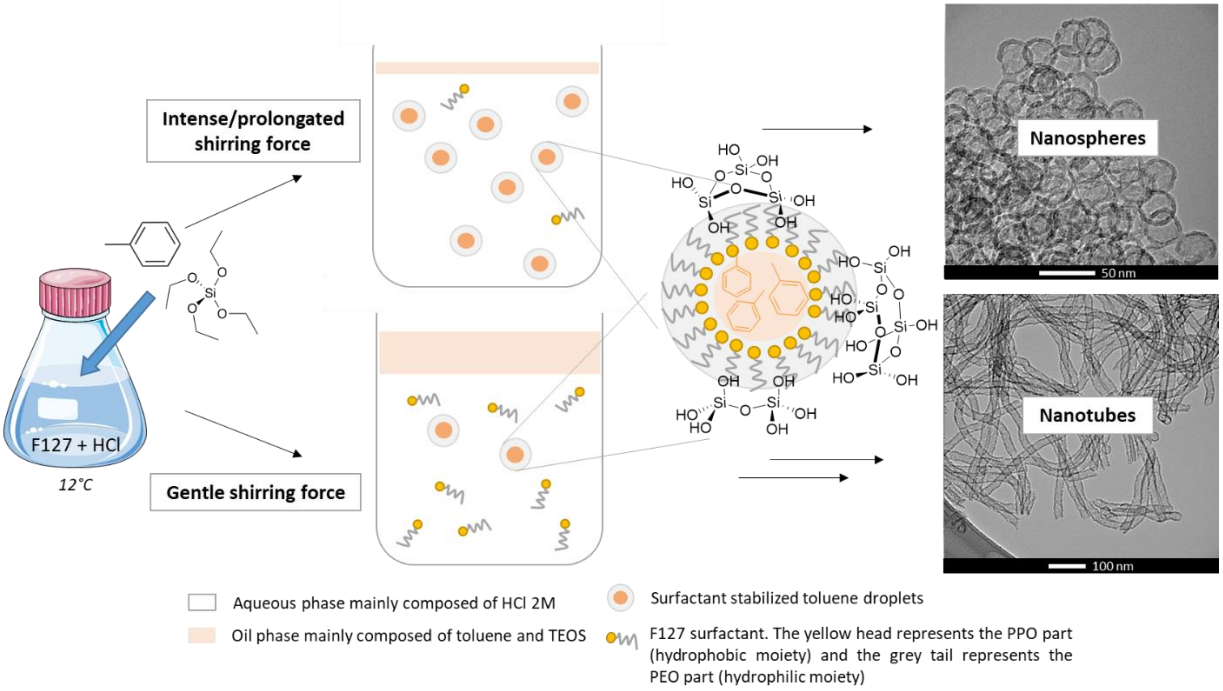

Figure 8 - The synthesis mixture is made of an oil phase mainly composed of toluene and TEOS and an acid aqueous phase. Through the stirring of the mixture, surfactant stabilized toluene droplets are created in the aqueous phase. If the shirring force is intense, a high quantity of toluene droplets can be found in the aqueous phase, leading to the formation of silica hollow nanospheres. If the shirring force is gentle, small amount of stabilized toluene droplets are created in the aqueous phase, inducing tubular structures in the final material.

To investigate if the addition of the silica precursor is responsible of the formation of tubular structures, a small fraction of the synthesis mixture at the step C (0 h, 250 rpm, Figure 1) was analyzed via TEM (dry state). Four hours after TEOS addition, the micrographs revealed the presence of a filamentous network from which separated cylindrical structures appear (Figure 9 a, b). The full development of the individual tubular structures was finally achieved after 24 h (Figure 9 c). Hence, the formation of cylindrical structures seems to be driven by the chemical reactions of the silica precursor, as structural changes occur simultaneously with the progression of TEOS hydrolysis/condensation. This phenomenon was already proposed in the case of SBA-15.[5] Here, the ethanol released after TEOS hydrolysis (3 mL) could play a major role in this transition by interacting with the hydrophilic part of the templating agent or with the hydroxylated silica species.

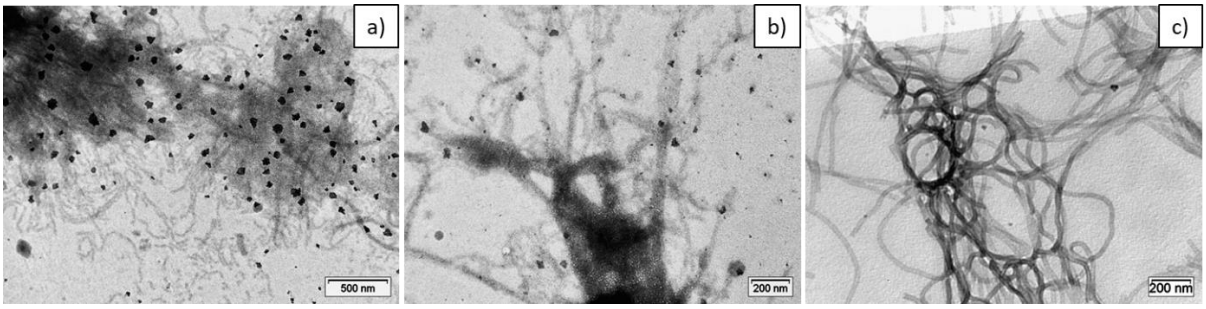

Figure 9 - TEM micrograph (dry state) of the reaction mixture 4 hours (a and b) and 24 hours (c) after the addition of TEOS.

From this study emerged that the stirring speed and time between the addition of toluene and TEOS induced changes in the synthesis mixture. In particular, the distribution of toluene within the aqueous phase of the mixture has a pivotal role for the formation of either tubular or spherical hollow nanostructures. This study aimed to extensively study the impact of two synthesis parameters although the change of morphology can be driven by other. For example, the temperature of synthesis or the use of various co-solvent and swelling agents as xylene, ethylbenzene, 1,3,5-triisopropylbenzene or cyclohexane have already shown to have an impact on the morphology of the resulting solid by affecting the solubilization of the oil phase in the micelles.[3, 41]

Nanotubes and nanospheres as vehicle for curcumin release

Silica-based nanotubes and nanospheres display promising textural properties for their application as vehicle for the release of an active pharmaceutical ingredient (API). Their exceptionally high pore volume (mostly due to the internal cavity) is expected to be highly convenient for the loading of an elevate API. Moreover, their large and accessible mesopores should also induce a rapid release of poorly soluble components, such as curcumin, here chosen as a relevant example of API. Nanospheres (NS) were initially selected to investigate the loading capacity of our materials via wet impregnation of 10, 20 and 30 wt% of curcumin (named NS-10, NS-20 and NS-30, respectively). Theoretical loadings were first verified via TGA and chemical combustion analysis. Experimental values (Table S1) were in excellent agreement with the theoretical ones, proving the efficiency of the loading procedure.

To confirm that the curcumin did not undergo major modifications of the structure during the step of impregnation, we turn our attention to solid-state (ss) nuclear magnetic resonance (NMR) spectroscopy.[42-44] Solid-state ^{13}C CP-MAS spectra of commercial curcumin together with the materials NT-10, NT-20 and NT-30 are shown in Figure S15. The resonances were assigned based on liquid state ^{13}C NMR spectrum (Figure S16) as well as of assignments already reported in the literature.[42, 45, 46] Regarding the spectra of commercial curcumin, different regions can be clearly distinguished. The two most deshielded

contributions appearing at *c.a.* 185 ppm can be ascribed to the carbon engaged in the carbonyl group. The contribution appearing at *c.a.* 150 ppm can be related to the presence of the quaternary C-OH/C-OCH_3 carbon atoms. The peaks appearing in the region located between 100 and 150 ppm can be ascribed to the -CH_2 contributions of the curcumin backbone. Finally, the two shielded contributions appearing at *c.a.* 55 ppm can be correlated to the presence of the -CH_3 groups of curcumin. The spectra of NS-10, NS-20 and NS-30 differ from the spectra of commercial curcumin, mainly in terms of peak width. The signals attributed to curcumin in the nanospheres are all broader than those observed for the commercial compound. This result indicates the presence of interactions of curcumin molecules with the surface of the silica nanospheres, leading to a certain decrease of crystallinity.

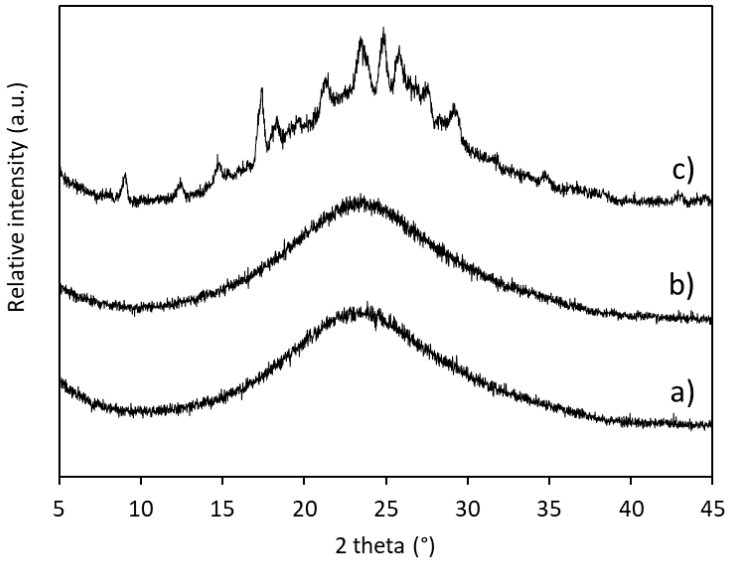

Figure 10 - PXRD of NS-10 (a), NS-20 (b) and NS-30 (c).

To confirm this hypothesis, the physical state of curcumin was investigated both before and after solvent evaporation via powder X-rays diffraction (PXRD). Wide angle PXRD patterns of commercial curcumin, nanospheres and their physical mixture were reported in Figure S17. Unlike pure commercial curcumin, NS-10 and NS-20 (Figure 10) did not display any sharp diffraction peak, indicating the amorphous nature of the samples. Nevertheless, the presence of finely dispersed crystallites of curcumin (smaller than the detection limit) cannot be excluded. NS-30 clearly shows the presence of intense reflections that can be attributed to crystalline curcumin species.[47]

Since the amorphous nature of loaded solids was already shown to be favorable for the release kinetic of API[18], silica nanotubes were impregnated with curcumin by following the same procedure and considering

a theoretical loading of 20 wt.%. The experimental loading, determined via TGA and CHN combustion analysis was in full agreement with the expected value (Table S1). Moreover, PXRD analysis confirmed the amorphous nature of the sample (see Figure S18). It is important to note that a curcumin loading of 20 wt% is an excellent achievement if compared to the values for mesoporous silica-based carriers already reported in literature.[48-50]

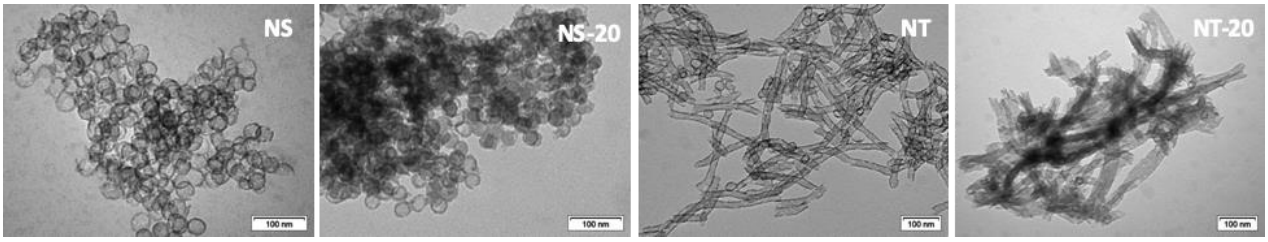

Figure 11 – TEM micrographs of nanospheres (NS) and nanotubes (NT) before and after curcumin impregnation (20 wt. %).

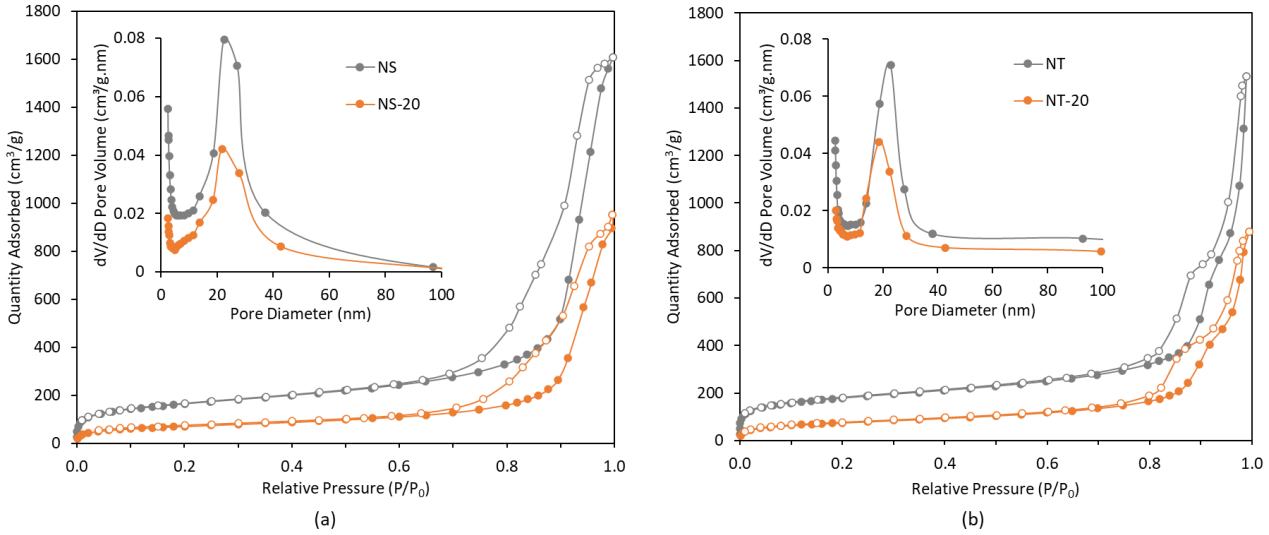

Figure 12 – N_2 adsorption-desorption isotherms and BJH-KJS pore size distribution of nanospheres (a) and nanotubes (b) before and after impregnation with curcumin.

Table 2 – Textural properties of nanospheres and nanotubes before and after impregnation.

Entry	Solid	BET SSA (m^2/g)	MPD BJH (nm)	V_t (cm^3/g)
1	NS	600	23	2.4
2	NS-20	280	22	2.0
3	NT	630	22	2.4
4	NT-20	320	19	1.1

The morphology of curcumin loaded nanospheres (NS-20) and nanotubes (NT-20) was investigated via transmission electron microscopy. TEM micrographs (Figure 11) show that both nanostructures preserve their original morphology without any visible damage. Moreover, it can be clearly seen that most particles show dark interiors. This lack of contrast can be associated to the presence of curcumin loaded into the internal void of spheres/tubes thus further proving the successful incorporation of curcumin within the silica nanostructures. The loading of nanotubes or nanospheres with curcumin did not result in any morphologic change but significantly modified the textural properties of the solids. N_2 adsorption-desorption isotherms of loaded solids (Figure 12) show a drastic decrease in the adsorbed amount of nitrogen, reflecting the decrease in the total pore volume of the carrier (compare entries 1 with 2 and 3 with 4 in Table 2). Both loaded solids are characterized by slightly reduced pore size when compared to the unloaded nanostructures. Curcumin loading strongly reduces the BET specific surface area of both materials (see Table 2). The reduction of pore volume and diameter further confirm the successful loading of curcumin mainly in the pores of nanotubes and nanospheres.

The release of curcumin from nanotubes and nanospheres was evaluated in simulated intestinal fluid (phosphate buffer saline, PBS, with pH 6.8) under sink conditions, created via the addition of 0.5 vol.% of Tween 80 in the medium.[51] Release tests were performed in duplicate. The in-vitro release profiles of NS-20 and NT-20 were illustrated in Figure 13 and compared to the dissolution rate of pure crystalline curcumin. After 30 min, NS-20 released an amount of curcumin equivalent to ~50 % of the initial drug loading. The curcumin release continues to proceed rapidly to reach *ca.* the 80 % in 2 h. Within 24 h of experiment, almost all the initial drug loading was released in the medium. The release of curcumin from NT-20 shows a similar profile than NS-20 with a slightly slower kinetic. The decrease of rate can be ascribed to the morphology of nanotubes and, in particular, to the length of the tubes probably decreasing the diffusion rate of curcumin to the release medium. In comparison, the dissolution rate of crystalline curcumin followed a distinct behavior. A dissolution of only ~10 % was measured after 30 min of experiment, which represents a quantity of curcumin in the medium 5-fold lower than the one measured for NS/NT-20. With the time, the dissolution of crystalline curcumin continues to slowly increase reaching ~60 % within 6 hours. Curcumin was totally dissolved in the medium within 24 hours.

To have a meaningful comparison among the different solids and correctly evaluate the dissolution rate of curcumin, a time within the period needed for human small intestine transit should be considered. Since the transit time is known to be about 3-4 hours[52], a time of 2 h could be reasonably selected as point of comparison. As can be clearly seen in Figure 13, after 2 hours of release experiment, the curcumin

available in the medium is ~3 time higher in the case of NT/NS-20 than for commercial curcumin. A similar trend is observed if the samples are compared after 4 h hence after a period corresponding to the higher transit time in human small intestine. The improved release kinetic of NS/NT-20 can be attributed to the presence of finely dispersed aggregates of amorphous curcumin into the widely open mesostructure of the carrier. On the one hand, the presence of amorphous curcumin should maximize the interactions with the release medium and hence, promote the dissolution of the active substance. On the other hand, the open structure of nanotubes and nanospheres should maximize the free diffusion of curcumin from their pores. Similar dissolution improvements were reported when comparing the dissolution of pure crystalline itraconazole to the release of itraconazole from ordered mesoporous silica.[25] The results emphasized the promising performances of silica nanotubes/spheres as carrier for curcumin delivery in simulated intestinal fluid conditions, where the dissolution of this active can otherwise be considered as slow.

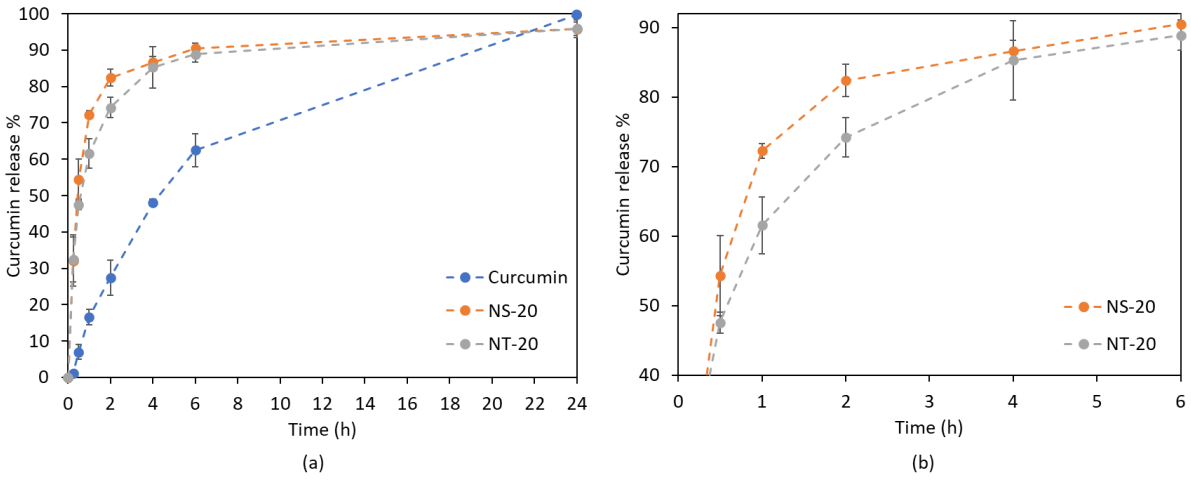

Figure 13 - Release profiles of curcumin, NS-20 and NT-20 in PBS pH 6.8 (0.5 vol.% of Tween 80) until 24h (a). Magnification of the release profiles of NS-20 and NT-20 in the region 0.5-6h (b). Release experiments were performed in duplicate.

To move further our investigation, release behavior of both NS-20 and NT-20 was compared to some of the most commonly reported silica-based materials. In particular, porous nanospheres (P-NS)[53] and large-pore SBA-15 (LP-SBA)[8] were selected to be impregnated with 20 wt.% of curcumin. The impregnated solids were called P-NS-20 and LP-SBA-20, respectively. P-NS was chosen to compare hollow nanospheres with spheres having a similar diameter but also an internal porous structure. LP-SBA was chosen to compare hollow nanotubes with a periodical structure made of tubes presenting a similar internal diameter.

The analysis of P-NS-20 and LP-SBA-20 shows the expected curcumin loading and the amorphous nature of the samples. The complete characterization of the supports both before and after impregnation can be found in supporting information (Figure S19-21, Table S2).

P-NS-20 and LP-SBA-20 both showed improved release kinetic behavior if compared to pure curcumin. The analysis of the release profile of both P-NS-20 and LP-SBA-20 reveals that *ca.* 70 % of the initial drug loading was release after 2 hours of experiments. This value is lower if compared to the amount of curcumin released from NS-20 or NT-20 at the same time (82 % and 74 % respectively). This difference can be attributed to the smaller pore diameter of porous nanospheres (in the case of P-NS-20) or to the more compact structure with longer channels (in the case of LP-SBA-20) that can decrease the release of curcumin in the PBS medium. At shorter time of the release experiment (Figure 14), NT-20 and NS-20 show improved release behavior compared to P-NS and LP-SBA. The improved release behavior at short time periods can be explained by the highly open structure of NT and NS. This characteristic is expected to favor the diffusion of curcumin from the surface of the solids to the external medium.

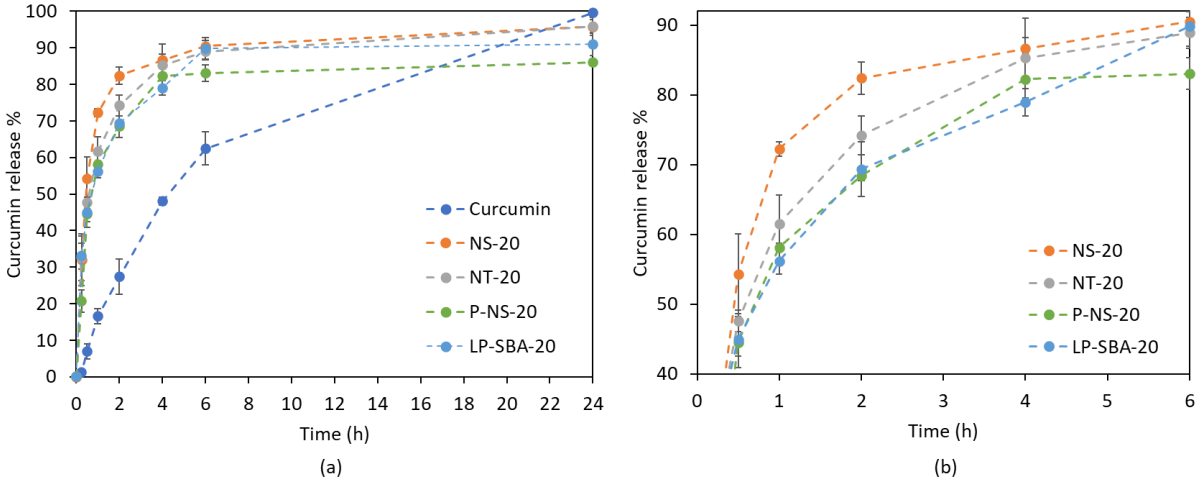

Figure 14 - Release profiles of curcumin, NS-20, NT-20, P-NS-20 and LP-SBA-20 in PBS pH 6.8 (0.5 vol.% of Tween 80) until 24h (a). and until 6h (b). Magnification of the release profiles of NS-20, NT-20, P-NS-20 and LP-SBA-20 in the region 0.5-6h. Release experiments were performed in duplicate.

CONCLUSION

The synthesis parameters guiding the development of nanotubes and nanospheres were investigated using the synthesis of silica nanotubes as reference and varying separately the stirring speed and the time between the addition of toluene and TEOS. To elucidate the global mechanism involved in the synthesis of both hollow nanostructures, a stepwise approach together with an in-depth characterization was

employed. The morphologies involved in the early-stage of material formation were observed thanks to liquid-phase transmission electron microscopy. We found that a gentle shearing force induces a low amount of toluene stabilized by F127 in the aqueous phase of the synthesis mixture. Toluene was found in the form of spherical droplets which were identified as template. In case of a small quantity of toluene droplets in the aqueous phase, the addition of the silica precursor (TEOS) induces the formation of cylindrical structures to finally lead to well-defined tubular morphology. When an intense/prolongated shearing force was applied, a higher amount of toluene was stabilized by the F127 surfactant inducing the creation of an elevated concentration of spherical droplets. The number of toluene droplets stabilized in the aqueous phase was identified as the key parameter guiding the development of hollow nanotubes or nanospheres. Since nanotubes and nanospheres showed elevate pore volume and highly accessible mesopores, their use as carrier for increasing the dissolution rate of the poorly water-soluble curcumin was investigated. A loading of 20 wt.% was chosen as the best compromise between a quantity high enough to enable the application in drug release while preserving the amorphous nature of the whole sample. Nanotubes as well as porous nanospheres (P-NS) and large-pore SBA-15 (LP-SBA) were loaded with the above-mentioned percentage of curcumin. The in-vitro dissolution experiment conducted in simulated intestinal fluid under sink conditions showed a clear enhancement of the dissolution rate of the loaded solids if compared to commercial curcumin. Moreover, nanotubes and nanospheres showed improved release behavior at short time when compared to P-NS and LP-SBA. The improved release behavior can be explained by the highly-open structure of nanotubes and nanospheres reducing diffusion limitation.

METHODS

Synthesis of silica nanotubes

Silica-based nanotubes were prepared adapting a previously reported method,[8] at a stirring speed of 250 rpm in a 250 mL covered glass container maintained at a temperature of 12 °C. The glass container was 70 mm in diameter and 133 mm in height and the stirring bar was 6 mm in diameter and 30 mm in length. 1.0 g (0.080 mmol) of Pluronic F127 was added to 60.0 mL of HCl 2 M. The mixture was stirred for one hour to ensure the complete solubilization of the templating agent. Then, a mixture of tetraethyl orthosilicate (TEOS - 2.8 g - 13 mmol) and toluene (3.0 mL - 0.028 mol) was prepared. This solution was added dropwise to the templating agent solution. After 24 hours stirring at 12 °C, the pH of the synthesis mixture was adjusted to the final value of 9, using 10.5 mL of concentrated ammonia solution (30 wt.%).

The reaction mixture was then stirred for one night (around 16 hours) at 12 °C. After filtration of the mixture and washing with distilled water, the obtained gel was lyophilized overnight. The collected white powder was finally calcined under air at 550 °C for 5 hours with a heating rate of 2 °C/min. The resulting solid was named (0 h, 250 rpm) to be consistent with the simultaneous addition of toluene and TEOS (0 h delay) and with the stirring speed used all along the procedure.

In the following section, the as-mentioned procedure was used as starting point. Only the modification(s) of the procedure was/were mentioned.

Investigation of different synthesis parameters for the preparation of hollow silica nanostructures

- *Delay time between the addition of toluene and TEOS*

The addition of toluene was separated from the addition of TEOS. In practice, after the solubilization of the templating agent at 12 °C (F127 - 1.0 g - 0.080 mmol), toluene (3.0 mL - 0.028 mmol) was added to the reaction mixture under 250 rpm stirring. After 2, 8 or 24 hours stirring at 12 °C, TEOS (2.8 g - 13 mmol) was added dropwise to the synthesis mixture while the stirring was maintained. The resulting solids were named according to the delay used between toluene and TEOS addition and to the stirring speed, namely (2 h, 250 rpm), (8 h, 250 rpm) and (24 h, 250 rpm).

- *Stirring speed*

The simultaneous addition of toluene and TEOS (0 h delay), used in section 2.1 was kept constant. The only difference is that the stirring speed was modified to 350 rpm, 450 rpm or 550 rpm all along the experiment. The resulting solids were named according to the delay used between toluene and TEOS addition and to the stirring speed, namely (0 h, 350 rpm), (0 h, 450 rpm) and (0 h, 550 rpm).

- *Stirring speed after the addition of TEOS*

After the solubilization of the templating agent at 12 °C (F127 - 1.0 g - 0.080 mmol), toluene (3.0 mL - 0.028 mmol) and TEOS (2.8 g - 13 mmol) were added dropwise to the reaction mixture in a simultaneously way under 250 rpm stirring. After 2 h, 4 h or 8 h of 250 rpm stirring, the stirring speed was increased to 550 rpm for 24 h.

- *Stirring speed before the addition of TEOS*

The templating agent (F127 - 1.0 g - 0.080 mmol) was solubilized at 12 °C for 1 hour under 1000 rpm. Then, toluene (3.0 mL - 0.028 mmol) was added dropwise to the mixture while the stirring was kept

constant. After 2 hours, the stirring speed was reduced to 250 rpm and TEOS (2.8 g - 13 mmol) was added dropwise to the synthesis mixture.

- *Synthesis without toluene*

After the solubilization of the templating agent (F127 - 1.0 g - 0.080 mmol) at 12 °C, 250 rpm, TEOS (2.8 g - 13 mmol) was added to the reaction mixture while the stirring was maintained for 24 h. Then, the steps described for the synthesis of Si-based nanotubes were followed.

- *Synthesis with a reduced amount of toluene*

After the solubilization of the templating agent (F127 - 1.0 g - 0.080 mmol) at 12 °C, 250 rpm, toluene (1.0 mL - 0.009 mmol) was added to the reaction mixture. The sol was stirred at 250 rpm for 24 h, after which TEOS (2.8 g - 13 mmol) was also added under stirring.

Synthesis of porous silica nanospheres

Porous nanospheres were synthesized according a procedure reported by Aprile et al.[53] CTAB (656.0 mg, 1.800 mmol) was dissolved in milli-Q water (314 ml, 17.4 mol) in a 1000 mL polypropylene bottle. After the complete dissolution of CTAB, ammonia (1.0 g, 8.6 mmol) was added dropwise. The solution was stirred for 30 min, then filtered and washed three times with milli-Q water and then with EtOH. The final solid was dried in the oven at 65 °C and then calcined at 550 °C for 6 hours with a heating rate of 3 °C/min. The resulting solid was named P-NS.

Synthesis of large-pore SBA-15

According a procedure reported by Kruk et al.,[8] LP-SBA was prepared at a stirring speed of 250 rpm in a 250 mL covered glass container maintained at a temperature of 12 °C. The glass container was 70 mm in diameter and 133 mm in height and the stirring bar was 6 mm in diameter and 30 mm in length. 1.0 g (0.080 mmol) of Pluronic F127 was added to 60.0 mL of HCl 2 M. The mixture was stirred for one hour to ensure the complete solubilization of the templating agent. Then, a mixture of tetraethyl orthosilicate (TEOS – 4.5 g - 22 mmol) and toluene (3.0 mL - 0.028 mol) was prepared. This solution was added dropwise to the templating agent solution. After 24 hours stirring at 12 °C, the mixture was transferred in a 250 mL polypropylene bottle and kept at 120 °C for 2 days. The resulting product was filtered and washed with distilled water. The powder was dried in the oven at 100 °C and then calcined at 550 °C for 5 hours with a heating rate of 2 °C/min. The resulting solid was named LP-SBA.

Impregnation of different silicates with curcumin

The impregnation of silica-based nanotubes, nanospheres, porous nanospheres and large pore SBA-15 was achieved via a wet-impregnation procedure. A solution of curcumin in acetone with a concentration equivalent to 4 g/L was prepared. The pores of the solid were evacuated through drying the samples overnight in a vacuum oven heated at 60 °C. 50.0 mg of the solid were introduced in a 10 mL round bottom flask. Then, the volume of curcumin solution needed to achieve 10, 20 or 30 wt.% of loading (1.39 mL, 3.13 mL and 5.35 mL, respectively) was added to the solid in the round bottom flask. The mixture was stirred during 15 hours at 400 rpm, protected from the light. The solvent was removed via rotary evaporation. The samples were dried overnight in the vacuum oven at 40 °C to ensure the full evaporation of acetone from the surface of the solid.

Characterization

Transmission electron microscopy (TEM) images were taken using a Philips Tecnai 10 microscope operating at 80 kV. High resolution TEM images were taken using a Philips Tecnai 20 operating at 200 kV. Nitrogen adsorption-desorption analyses were carried out at 77 K with a volumetric adsorption analyzer (Micromeritics ASAP 2420). Prior to the analysis, the samples were pre-treated 12 hours at 170 °C under reduced pressure (0.1 mbar). For impregnated solid, the samples were pre-treated 8 hours at 120 °C. The Brunauer–Emmet–Teller (BET) method was applied in the 0.05-0.20 P/P_0 range to calculate the specific surface area, while the pore size distributions were calculated from the adsorption branch of the isotherm using the Barrett–Joyner–Halenda (BJH) method with the Kruk-Jaroniec-Sayari (KJS) correction.

Dynamic light scattering (DLS) experiments were performed at 12°C on a NanoPlus HD nanoparticles analyzer. The scattering angle was 165° (back-scattering) and the light source was a semi-conductor laser diode (70 mW, 660 nm).

For liquid-phase TEM (LP-TEM), samples were collected from the aqueous phase of the reaction mixture (main phase) thanks to a syringe. The samples were passed through a 0.45 µm PTFE syringe filter to remove any dust or large aggregates. The samples were loaded in a Si-based microchannel device with a SiN_3 windows (300 um length, 25 um width). The compatibility of the liquid-cell system with toluene and HCl 2 M was previously confirmed. One droplet of the sample was pushed in the Si-based liquid cell through capillarity forces. The liquid cell was then sealed and mounted on a copper grid. The liquid-cell integrity was verified by pumping the holder under vacuum. Note that there is 30 min delay between the time the cell holder is prepared and the time it is imaged. The specimens were imaged with a Philips Tecnai 20 operating at 200 kV with a spot size of 5 to minimize the effect of the electron beam on the samples. At any time of the sample analysis, the electron dose was below 0.01 $e^-/Å.s$.

Quantitative ^{1}H NMR spectra were recorded without sample spinning, using a 400 MHz spectrometer operating at 12 °C, equipped with a 5-mm broadband probe and temperature regulation. ^{1}H NMR spectra were recorded using the presat pulse sequence and following acquisition parameters: relaxation delay of 10 s, presaturation delay of 5 s, acquisition time of 5 s, excitation pulse of 90 ° and 8 transients. D_2O was used for the ^{2}H lock. The ^{1}H chemical shift was referenced to water signal (4.79 ppm) or TMS (0.0 ppm), which were used as internal reference.

Powder X-ray diffraction (XRD) patterns were recorded on a PANalytical X'pert diffractometer with Cu Kα radiation (k = 1.54178 Å). Thermogravimetric analyses (TGA) were performed on a Mettler Toledo TGA/DSC 3^{+} STARe System. The samples were analyzed using a temperature ramp from 30 °C to 800 °C at 10 °C/min under air flow (60 mL/min). Chemical combustion analyses (CHN) were performed on a Perkin-Elmer 2400 Serie 2 analyzer.

Solid state ^{13}C CP-MAS NMR spectra were recorded at room temperature, on a Jeol ECZ-R 600 MHz spectrometer operating at 14.1 T, using a contact time of 2 ms, a spinning rate of 8 KHz and an automas probe of 3.2 mm.

Curcumin release experiments

The release experiments were performed in duplicate in simulated intestinal fluid (phosphate buffer saline, PBS, pH = 6.8) heated thanks to a water bath maintained at 37 °C. All dissolution experiments were performed in sink conditions, created via the addition of 0.5 vol.% of Tween 80 in the release medium. The impregnated solid (with a mass corresponding to 1 mg of curcumin) was suspended in 80.0 mL of simulated intestinal fluid. At specific intervals (from 15 min to 24 h), 2 mL of release medium was collected and an equal amount of fresh simulated intestinal fluid was added. The withdrawn sample was centrifuged 10 min at 4500 rpm. Prior to the analysis via UV-vis, the supernatant was diluted with methanol (1.5: 1). The concentration of curcumin in the samples was deducted measuring the absorbance of the solutions using UV-visible spectrometry at a wavelength of 430 nm.

CONFLICTS OF INTEREST

There are no conflicts of interest to declare.

ACKNOWLEDGEMENTS

Authors acknowledge the FNRS for the financial support including via the research project grant G 4/1/6-GEQ/CDB. L. Soumoy thanks the FNRS for the financial support in the context of her FRIA PhD grant. This research used resources of PC2 (Plateforme Technologique Physico-Chemical Characterization) and MORPH-IM (Morphology & Imaging) technology platforms located at the University of Namur.

ASSOCIATED CONTENT

Supporting information available: N_2 adsorption-desorption isotherms, pore size distributions, schemes with conditions of synthesis, DLS, TEM images, table with physico-chemical properties, liquid-sate NMR, solid-state TOSS CP MAS NMR, PXRD.

REFERENCES

1. Pal, N.; Lee, J.-H.; Cho, E.-B., Recent trends in morphology-controlled synthesis and application of mesoporous silica nanoparticles. *Nanomaterials* **2020,** *10* (11).

2. Beaton, L.; Zhang, S.; Kruk, M., Formation of double-helical structures by silica nanotubes templated by mixtures of common nonionic surfactants in aqueous solutions. *ACS Nano* **2021,** *15* (1), 1016-1029.

3. Li, Y.; Kruk, M., Single-micelle-templated synthesis of hollow silica nanospheres with tunable pore structures. *RSC Advances* **2015,** *5* (85), 69870-69877.

4. Huang, L.; Kruk, M., Synthesis of ultra-large-pore FDU-12 silica using ethylbenzene as micelle expander. *Journal of Colloid and Interface Science* **2012,** *365* (1), 137-142.

5. Flodström, K.; Wennerström, H.; Alfredsson, V., Mechanism of mesoporous silica formation. A time-resolved NMR and TEM study of silica−block copolymer aggregation. *Langmuir* **2004,** *20* (3), 680-688.

6. Febriyanti, E.; Suendo, V.; Mukti, R. R.; Prasetyo, A.; Arifin, A. F.; Akbar, M. A.; Triwahyono, S.; Marsih, I. N.; Ismunandar, Further insight into the definite morphology and formation mechanism of mesoporous silica KCC-1. *Langmuir* **2016,** *32* (23), 5802-5811.

7. Suteewong, T.; Sai, H.; Bradbury, M.; Estroff, L. A.; Gruner, S. M.; Wiesner, U., Synthesis and formation mechanism of aminated mesoporous silica nanoparticles. *Chemistry of Materials* **2012,** *24* (20), 3895-3905.

8. Huang, L.; Kruk, M., Versatile surfactant/swelling-agent template for synthesis of large-pore ordered mesoporous silicas and related hollow nanoparticles. *Chemistry of Materials* **2015,** *27* (3), 679-689.

9. Soumoy, L.; Célis, C.; Debecker, D. P.; Armandi, M.; Fiorilli, S.; Aprile, C., Hafnium-doped silica nanotubes for the upgrading of glycerol into solketal: Enhanced performances and in-depth structure-activity correlation. *Journal of Catalysis* **2022,** *411*, 41-53.

10. Bivona, L. A.; Vivian, A.; Fusaro, L.; Fiorilli, S.; Aprile, C., Design and catalytic applications of 1D tubular nanostructures: Improving efficiency in glycerol conversion. *Applied Catalysis B: Environmental* **2019,** *247*, 182-190.

11. Loverde, S. M.; Ortiz, V.; Kamien, R. D.; Klein, M. L.; Discher, D. E., Curvature-driven molecular demixing in the budding and breakup of mixed component worm-like micelles. *Soft Matter* **2010,** *6* (7), 1419-1425.

12. Mellaerts, R.; Aerts, C. A.; Humbeeck, J. V.; Augustijns, P.; den Mooter, G. V.; Martens, J. A., Enhanced release of itraconazole from ordered mesoporous SBA-15 silica materials. *Chemical Communications* **2007,** (13), 1375-1377.

13. Heikkilä, T.; Salonen, J.; Tuura, J.; Hamdy, M. S.; Mul, G.; Kumar, N.; Salmi, T.; Murzin, D. Y.; Laitinen, L.; Kaukonen, A. M.; Hirvonen, J.; Lehto, V. P., Mesoporous silica material TUD-1 as a drug delivery system. *International Journal of Pharmaceutics* **2007,** *331* (1), 133-138.

14. Bagheri, E.; Ansari, L.; Abnous, K.; Taghdisi, S. M.; Charbgoo, F.; Ramezani, M.; Alibolandi, M., Silica based hybrid materials for drug delivery and bioimaging. *Journal of Controlled Release* **2018,** *277*, 57-76.

15. Kwon, S.; Singh, R. K.; Perez, R. A.; Abou Neel, E. A.; Kim, H.-W.; Chrzanowski, W., Silica-based mesoporous nanoparticles for controlled drug delivery. *Journal of Tissue Engineering* **2013,** *4*.

16. Hadipour Moghaddam, S. P.; Mohammadpour, R.; Ghandehari, H., In vitro and in vivo evaluation of degradation, toxicity, biodistribution, and clearance of silica nanoparticles as a function of size, porosity, density, and composition. *Journal of Controlled Release* **2019,** *311-312*, 1-15.

17. Bhavsar, D.; Patel, V.; Sawant, K., Systematic investigation of in vitro and in vivo safety, toxicity and degradation of mesoporous silica nanoparticles synthesized using commercial sodium silicate. *Microporous and Mesoporous Materials* **2019,** *284*, 343-352.

18. Maleki, A.; Kettiger, H.; Schoubben, A.; Rosenholm, J. M.; Ambrogi, V.; Hamidi, M., Mesoporous silica materials: from physico-chemical properties to enhanced dissolution of poorly water-soluble drugs. *Journal of Controlled Release* **2017,** *262*, 329-347.

19. Barros, C. H. N.; Casey, E., A review of nanomaterials and technologies for enhancing the antibiofilm activity of natural products and phytochemicals. *ACS Applied Nano Materials* **2020,** *3* (9), 8537-8556.

20. Joe, B.; Vijaykumar, M.; Lokesh, B. R., Biological properties of curcumin-cellular and molecular mechanisms of action. *Critical Reviews in Food Science and Nutrition* **2004,** *44* (2), 97-111.

21. Tran, P.; Pyo, Y.-C.; Kim, D.-H.; Lee, S.-E.; Kim, J.-K.; Park, J.-S., Overview of the manufacturing methods of solid dispersion technology for improving the solubility of poorly water-soluble drugs and application to anticancer drugs. *Pharmaceutics* **2019,** *11* (3).

22. McCarthy, C. A.; Ahern, R. J.; Dontireddy, R.; Ryan, K. B.; Crean, A. M., Mesoporous silica formulation strategies for drug dissolution enhancement: a review. *Expert Opinion on Drug Delivery* **2016,** *13* (1), 93-108.

23. Blagden, N.; de Matas, M.; Gavan, P. T.; York, P., Crystal engineering of active pharmaceutical ingredients to improve solubility and dissolution rates. *Advanced Drug Delivery Reviews* **2007,** *59* (7), 617-630.

24. Sathisaran, I.; Dalvi, S. V., Engineering cocrystals of poorly water-soluble drugs to enhance dissolution in aqueous medium. *Pharmaceutics* **2018,** *10* (3), 108.

25. Mellaerts, R.; Mols, R.; Jammaer, J. A. G.; Aerts, C. A.; Annaert, P.; Van Humbeeck, J.; Van den Mooter, G.; Augustijns, P.; Martens, J. A., Increasing the oral bioavailability of the poorly water soluble drug itraconazole with ordered mesoporous silica. *European Journal of Pharmaceutics and Biopharmaceutics* **2008,** *69* (1), 223-230.

26. Bukara, K.; Schueller, L.; Rosier, J.; Martens, M. A.; Daems, T.; Verheyden, L.; Eelen, S.; Van Speybroeck, M.; Libanati, C.; Martens, J. A.; Van Den Mooter, G.; Frérart, F.; Jolling, K.; De Gieter, M.; Bugarski, B.; Kiekens, F., Ordered mesoporous silica to enhance the bioavailability of poorly water-soluble drugs: Proof of concept in man. *European Journal of Pharmaceutics and Biopharmaceutics* **2016,** *108*, 220-225.

27. Kruk, M.; Jaroniec, M.; Sayari, A., Application of Large Pore MCM-41 Molecular Sieves To Improve Pore Size Analysis Using Nitrogen Adsorption Measurements. *Langmuir* **1997,** *13* (23), 6267-6273.

28. Ke, F.; Yi, J.; Zhang, S.; Zhou, S.; Ravikovitch, P. I.; Kruk, M., Structures and dimensions of micelle-templated nanoporous silicas derived from swollen spherical micelles of temperature-dependent size. *Journal of Colloid and Interface Science* **2019,** *544*, 312-320.

29. Gong, L.; Liao, G.; Luan, H.; Chen, Q.; Nie, X.; Liu, D.; Feng, Y., Oil solubilization in sodium dodecylbenzenesulfonate micelles: New insights into surfactant enhanced oil recovery. *Journal of Colloid and Interface Science* **2020,** *569*, 219-228.

30. Rao, J.; McClements, D. J., Lemon oil solubilization in mixed surfactant solutions: Rationalizing microemulsion & nanoemulsion formation. *Food Hydrocolloids* **2012,** *26* (1), 268-276.

31. He, Y.; Li, Z.; Simone, P.; Lodge, T. P., Self-assembly of block copolymer micelles in an ionic liquid. *Journal of the American Chemical Society* **2006,** *128* (8), 2745-2750.

32. Rowan, S. J., 100th anniversary of macromolecular science viewpoints. *ACS Macro Letters* **2021,** *10* (4), 466-468.

33. He, K.; Shokuhfar, T.; Shahbazian-Yassar, R., Imaging of soft materials using in situ liquid-cell transmission electron microscopy. *Journal of Physics: Condensed Matter* **2019,** *31* (10), 103001.

34. Zhu, C.; Liang, S.; Song, E.; Zhou, Y.; Wang, W.; Shan, F.; Shi, Y.; Hao, C.; Yin, K.; Zhang, T.; Liu, J.; Zheng, H.; Sun, L., In-situ liquid cell transmission electron microscopy investigation on oriented attachment of gold nanoparticles. *Nature Communications* **2018,** *9* (1), 421.

35. De Yoreo, J. J.; N. A. J. M, S., Investigating materials formation with liquid-phase and cryogenic TEM. *Nature Reviews Materials* **2016,** *1* (8), 16035.

36. Early, J. T.; Yager, K. G.; Lodge, T. P., Direct observation of micelle fragmentation via in situ liquid-phase transmission electron microscopy. *ACS Macro Letters* **2020,** *9* (5), 756-761.

37. Brinker, C. J.; Keefer, K. D.; Schaefer, D. W.; Assink, R. A.; Kay, B. D.; Ashley, C. S., Sol-gel transition in simple silicates II. *Journal of Non-Crystalline Solids* **1984,** *63* (1), 45-59.

38. Shen, D.; Yang, J.; Li, X.; Zhou, L.; Zhang, R.; Li, W.; Chen, L.; Wang, R.; Zhang, F.; Zhao, D., Biphase stratification approach to three-dimensional dendritic biodegradable mesoporous silica nanospheres. *Nano Letters* **2014,** *14* (2), 923-932.

39. Wang, W.; Wang, P.; Tang, X.; Elzatahry, A. A.; Wang, S.; Al-Dahyan, D.; Zhao, M.; Yao, C.; Hung, C.-T.; Zhu, X.; Zhao, T.; Li, X.; Zhang, F.; Zhao, D., Facile synthesis of uniform virus-like mesoporous silica nanoparticles for enhanced cellular internalization. *ACS Central Science* **2017,** *3* (8), 839-846.

40. Kelts, L. W.; Effinger, N. J.; Melpolder, S. M., Sol-gel chemistry studied by 1H and 29Si nuclear magnetic resonance. *Journal of Non-Crystalline Solids* **1986,** *83* (3), 353-374.

41. Fatieiev, Y.; Croissant, J. G.; Alamoudi, K.; Khashab, N. M., Cellular internalization and biocompatibility of periodic mesoporous organosilica nanoparticles with tunable morphologies: from nanospheres to nanowires. *ChemPlusChem* **2017,** *82* (4), 631-637.

42. Pöppler, A.-C.; Lübtow, M. M.; Schlauersbach, J.; Wiest, J.; Meinel, L.; Luxenhofer, R., Loading-dependent structural model of polymeric micelles encapsulating curcumin by solid-state NMR spectroscopy. *Angewandte Chemie International Edition* **2019,** *58* (51), 18540-18546.

43. Azaïs, T.; Tourné-Péteilh, C.; Aussenac, F.; Baccile, N.; Coelho, C.; Devoisselle, J.-M.; Babonneau, F., Solid-state NMR study of ibuprofen confined in MCM-41 material. *Chemistry of Materials* **2006,** *18* (26), 6382-6390.

44. Azaïs, T.; Laurent, G.; Panesar, K.; Nossov, A.; Guenneau, F.; Sanfeliu Cano, C.; Tourné-Péteilh, C.; Devoisselle, J.-M.; Babonneau, F., Implication of water molecules at the silica–ibuprofen interface in silica-based drug delivery systems obtained through incipient wetness impregnation. *The Journal of Physical Chemistry C* **2017,** *121* (48), 26833-26839.

45. Matlinska, M. A.; Wasylishen, R. E.; Bernard, G. M.; Terskikh, V. V.; Brinkmann, A.; Michaelis, V. K., Capturing elusive polymorphs of curcumin: a structural characterization and computational study. *Crystal Growth & Design* **2018,** *18* (9), 5556-5563.

46. Kong, X.; Brinkmann, A.; Terskikh, V.; Wasylishen, R. E.; Bernard, G. M.; Duan, Z.; Wu, Q.; Wu, G., Proton probability distribution in the O···H···O low-barrier hydrogen bond: a combined solid-state NMR and quantum chemical computational study of dibenzoylmethane and curcumin. *The Journal of Physical Chemistry B* **2016,** *120* (45), 11692-11704.

47. Sanphui, P.; Goud, N. R.; Khandavilli, U. B. R.; Bhanoth, S.; Nangia, A., New polymorphs of curcumin. *Chemical Communications* **2011,** *47* (17), 5013-5015.

48. Kotcherlakota, R.; Barui, A. K.; Prashar, S.; Fajardo, M.; Briones, D.; Rodríguez-Diéguez, A.; Patra, C. R.; Gómez-Ruiz, S., Curcumin loaded mesoporous silica: an effective drug delivery system for cancer treatment. *Biomaterials Science* **2016,** *4* (3), 448-459.

49. Cheng, C.-S.; Liu, T.-P.; Chien, F.-C.; Mou, C.-Y.; Wu, S.-H.; Chen, Y.-P., Codelivery of plasmid and curcumin with mesoporous silica nanoparticles for pomoting nurite outgrowth. *ACS Applied Materials & Interfaces* **2019,** *11* (17), 15322-15331.

50. Barros, C. H. N.; Devlin, H.; Hiebner, D. W.; Vitale, S.; Quinn, L.; Casey, E., Enhancing curcumin's solubility and antibiofilm activity via silica surface modification. *Nanoscale Advances* **2020,** *2* (4), 1694-1708.

51. Klein, S., The use of biorelevant dissolution media to forecast the in vivo performance of a drug. *The AAPS Journal* **2010,** *12* (3), 397-406.

52. DeSesso, J. M.; Jacobson, C. F., Anatomical and physiological parameters affecting gastrointestinal absorption in humans and rats. *Food and Chemical Toxicology* **2001,** *39* (3), 209-228.

53. Godard, N.; Collard, X.; Vivian, A.; Bivona, L. A.; Fiorilli, S.; Fusaro, L.; Aprile, C., Rapid room temperature synthesis of tin-based mesoporous solids: Influence of the particle size on the production of ethyl lactate. *Applied Catalysis A: General* **2018,** *556*, 73-80.

TOC Graphic

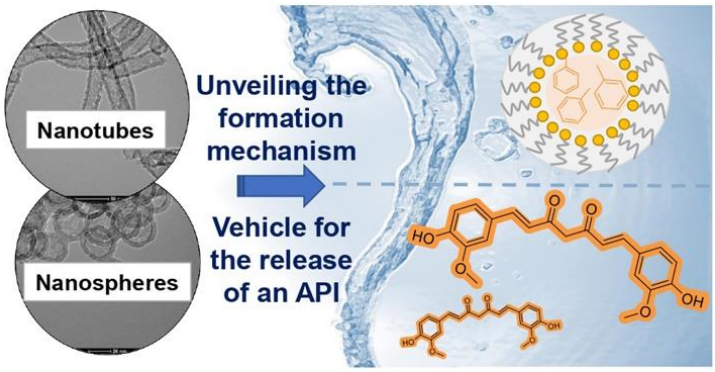
Nanotubes
Nanospheres
Unveiling the formation mechanism
Vehicle for the release of an API
HO
O
O
O
OH